E-ISSN: 2788-9297
P-ISSN: 2788-9289
www.agrijournal.org
SAJAS 2024; 4(2): 101-108
Received: 28-05-2024
Accepted: 10-07-2024

Hussein Saeb Al-Khaiqani
Department of Soil and Water Sciences, Faculty of Agriculture, Kufa University, Iraq

Ayad Kadhim Ali Al-Husseni
Department of Soil and Water Sciences, Faculty of Agriculture, Kufa University, Iraq

Correspondence Author:
Hussein Saeb Al-Khaiqani
Department of Soil and Water Sciences, Faculty of Agriculture, Kufa University, Iraq

The impact of climate elements on the surface area of Sawa Lake using remote sensing data

Hussein Saeb Al-Khaiqani and Ayad Kadhim Ali Al-Husseni

Abstract
Sawa Lake is a significant historical and environmental landmark, with unique characteristics that have elevated it to the status of global natural heritage. The lake has changed dramatically over the last decade, resulting in a considerable drop in surface area. The current study employs remote sensing data and meteorological observations from 1994 to 2024 to investigate and analyze the likely causes of the region's significant fall in water levels. The MNDWI index showed that Lake Sawa's surface area increased in 1994, 2004, and 2014, reaching 4.31, 4.39, and 4.55 km². Between 2014 and 2024, the lake's area declined by 4.00 km², with the lowest reported surface area being 0.31 km² in 2024. This suggests that the lake's surface area decreased by more than 92% during the research. To better understand the potential causes of this reduction, additional research into climate changes and their impact on the region was accomplished. The climate change analysis for the periods 1994-2003, 2004-2013, and 2014-2023 noticed that temperature was the most significant changing factor, with an upward trend. The average minimum and maximum temperatures for the three periods were [(17.23, 32.68), (17.88, 32.72), and (19.04, 33.31)] °C, respectively. This temperature rise coincided with the lake's deterioration, thereby contributing to its surface area reduction through increased water losses owing to evaporation and higher water consumption for agricultural operations in the region, which increased by 238%. Because the region's primary water source is groundwater, the number of wells required to cover the water shortfall increased, resulting in higher water extraction rates. This lowered local groundwater thresholds and reduced levels in locations that rely on natural water flow, such as Lake Sawa, raising concerns that the lake may dry up and perish in the future years.

Keywords: Sawa Lake, remote sensing, climate elements, drought, surface area

1. Introduction
Drought is a natural phenomenon that has received a lot of attention from climate and hydrology scientists in the last 20 years [1]. Drought is generally caused by decreasing rainfall and rising temperatures [2]. The current study focused on Lake Sawa, one of the world's most distinctive lakes. It is a closed lake in southwestern Iraq, administratively inside the Al-Muthanna Governorate and 25 kilometers west of Samawah. The lake has no watercourse flowing into or out of it, relying instead on springs and groundwater that seep into it via cracks and faults beneath it from the Dammam and Umm er Radhuma aquifers [3]. The lake's water levels have dropped substantially in recent years, and the cause of the dip, as well as the reduced discharge from the feeding springs, is unknown [4].
Groundwater exploitation has risen over the last two decades to compensate for surface water deficits caused by climate change and decreasing flows in key rivers. As a result, the number of wells drilled in Iraq has increased, and enhanced extraction has caused groundwater levels to fall by more than 2 meters in central and southern Iraq, particularly in the southern desert [5]. Climate change is anticipated to reduce rainfall by 6% between 2020 and 2050, resulting in a 1.8 to 4.8-meter drop in groundwater levels in the higher aquifers during the following 31 years [6]. Drought monitoring on a regional and temporal scale is a complex procedure that has evolved over decades [7]. Drought indices are employed to track and identify drought conditions and other factors that contribute to water scarcity [8].
Recently, spectral indices have been employed to monitor droughts by detecting changes in lake surface areas [9]. Remote sensing has been used extensively to identify, map, analyze, and track drought and its consequences on surface and groundwater resources, particularly in resource-constrained places. Various high and medium spatial resolution remote sensing pictures have been utilized to track the drying of inland surface water bodies [10]. In Iraq, major efforts have been made to monitor the impact of drought on surface water bodies by extracting changes in surface water areas using remote sensing data [11].

However, inland water bodies are prone to dynamic changes caused by climate factors such as rising temperatures and decreased rainfall [12]. Furthermore, in some places near lakes such as Lake Sawa, agricultural lands that rely mostly on groundwater for irrigation are expanding [13].

Because the lake is located in a desert location demonstrated by drought and high summer temperatures, the seasonal need for water grows as temperatures rise to fulfill the needs of agricultural lands [14]. This, together with climate change, increases pressure on groundwater flows towards the lake. Climate change, particularly rising temperatures and fluctuating rainfall, presents a serious challenge to the region [15]. As a result, the research pursues to identify the specific factors that have harmed Lake Sawa and resulted in an exceptional loss in its water levels, in order to aid decision-makers in establishing a strategic approach to restore the lake based on the actual causes of the water level decline.

2. Study Are

The research area, Lake Sawa, is geographically situated in the southwestern region of Iraq, administratively within Al-Muthanna Governorate, and 25 km southwest of the center of Samawah city. It is located in a transitional zone between the western desert plateau and the alluvial plain. To the east and northeast, it is surrounded by the Al-Atshan River (a tributary of the Euphrates River), with the nearest point being 4 km distant. To the south, it is surrounded by the Samawah Salt Flats, about 7 km away. To the west and southwest, it is flanked by the boundary of the floodplain. Additionally, the area is bounded by belts of sand dunes to the east and west [16]. Astronomically, it is located between latitudes (44°59'29" and 45°01'46") and longitudes (31°17'43" and 31°19'80"), corresponding to path (168) and row (38) as spatial coordinates for the Landsat satellite [17] (Figure 1).

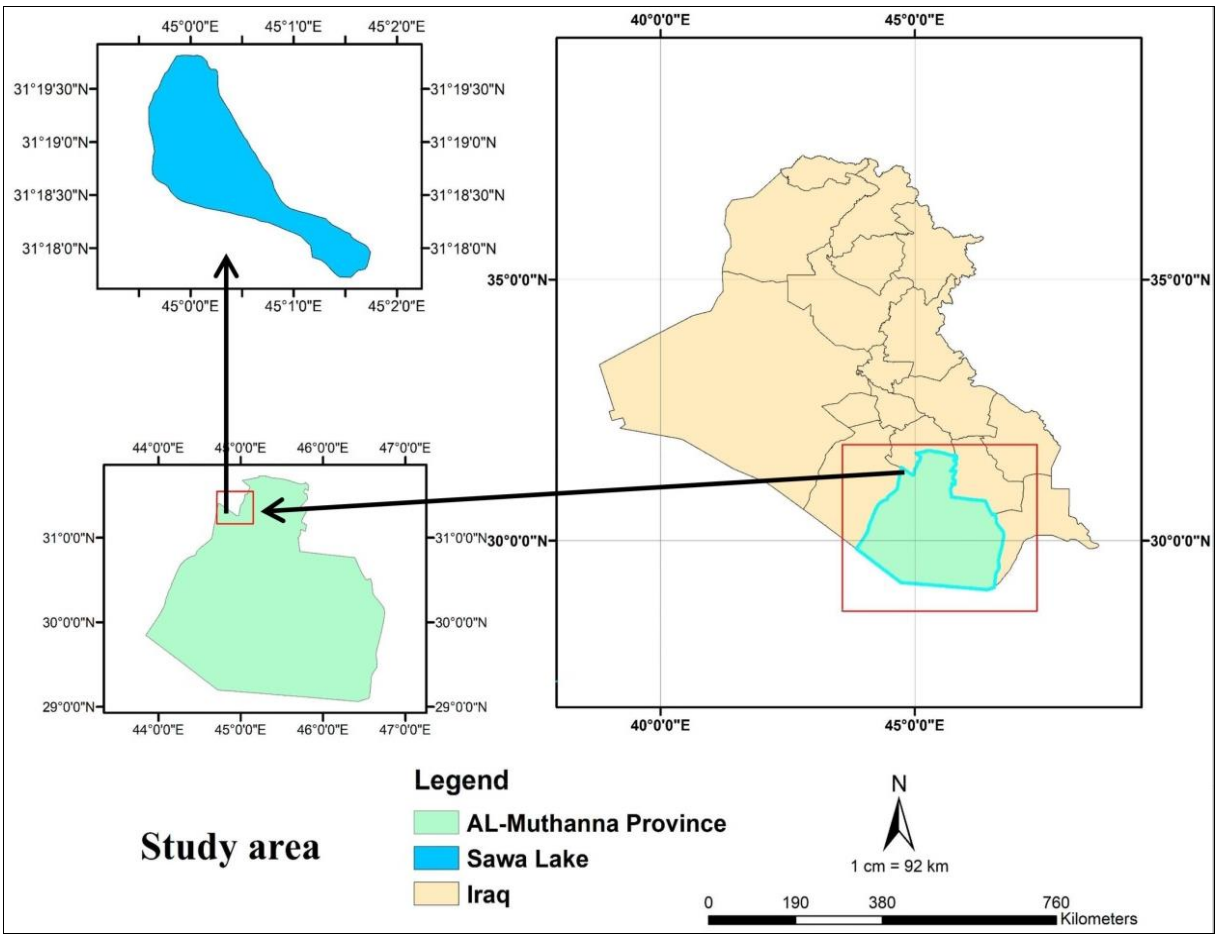

Fig 1: The location of the study area

3. Materials and Methods

3.1. Materials

In this study, remote sensing data from 1994 to 2024 and climate data from Samawah Meteorological Station from 1994 to 2023 were integrated to analyze the impact of climate changes in the study area on the water dynamics of Sawa Lake.

3.1.1. Remote sensing data used in the study

Landsat imagery from satellites were utilized in this study to map the path (168) and row (38) that included the subject region. The images were obtained from the US Geological Survey (USGS) website and comprise four satellite representations (Table 1) taken in February 1994, 2004, 2014, and 2024.

Table 1: Satellite images data

Years	Spacecraft ID	Sensor	Path/Row	Date
1994	Landsat 5	TM	168/38	12/2/1994
2004	Landsat 7	ETM+	168/38	17/2/2004
2014	Landsat 8	OLI	168/38	11/2/2014
2024	Landsat 9	OLI-2	168/38	19/2/2024

3.1.2. Climate Elements data

Table 2: Climatic elements of the study area from 1994 to 2023.

Years	Solar Brightness h d^{-1}	Temperature °C		Wind Speed m s^{-1}	Total Rainfall mm	Relative Humidity %	Atmospheric Pressure mbar
		Min.	Max.				
1994	8.75	16.95	31.87	2.31	120.91	44.00	1010.97
1995	9.03	16.59	31.62	2.84	136.80	43.16	1011.71
1996	8.71	17.79	32.70	3.02	116.50	43.00	1010.60
1997	8.93	16.36	31.63	2.62	163.12	43.83	1011.70
1998	8.80	17.49	33.06	2.25	65.60	42.91	1011.42
1999	8.55	16.94	33.05	2.83	83.30	39.91	1010.93
2000	8.20	16.79	32.18	4.11	115.00	39.25	1010.65
2001	8.05	16.81	34.69	4.60	76.20	39.08	1010.67
2002	7.96	17.57	33.49	4.13	82.61	37.66	1008.31
2003	7.95	19.01	32.57	2.80	163.12	40.83	1009.47
2004	8.27	16.55	33.35	3.16	35.00	38.91	1008.89
2005	8.50	16.89	33.11	3.31	119.01	38.50	1009.56
2006	8.08	18.43	32.30	3.80	165.90	41.41	1010.42
2007	9.01	17.86	32.20	4.30	62.30	37.66	1010.69
2008	8.70	18.08	32.78	3.13	56.00	36.00	1011.05
2009	8.35	18.47	32.53	3.07	54.11	36.58	1011.60
2010	8.80	19.01	33.44	3.20	47.01	38.00	1010.75
2011	9.40	18.38	32.15	3.26	58.42	37.25	1010.85
2012	9.23	18.77	33.09	3.63	118.40	34.33	1010.80
2013	9.66	16.45	32.30	3.50	147.82	38.75	1010.78
2014	8.89	16.56	31.65	3.45	114.10	38.00	1011.59
2015	9.21	19.01	33.77	3.71	115.40	37.91	1011.72
2016	8.99	18.99	33.70	3.77	147.30	37.33	1012.00
2017	9.77	18.45	33.69	3.25	102.80	39.41	1011.80
2018	9.50	19.96	33.10	3.84	163.09	37.58	1011.26
2019	9.41	19.35	32.62	3.95	114.38	39.33	1011.55
2020	9.39	19.40	33.50	4.58	119.91	34.58	1011.39
2021	9.20	19.45	34.12	4.36	31.47	30.91	1010.65
2022	8.15	19.35	33.75	4.32	161.35	32.00	1010.45
2023	9.26	19.90	33.22	3.42	133.65	35.66	1011.33

3.2. Methods

3.2.1. Study area clipping

The process of cutting and establishing the study area is one of the most important processes in the study since it works to reduce data and include processing and analysis operations just within the study area, thereby speeding up digital processing and shortening the time required. The clipping was performed utilizing the "Extract by Mask" tool of ArcGIS Pro's Arc Toolbox.

3.2.2. Pre-Processing of the satellite images

Before utilizing the image analysis functions on the selected satellite image, it should be prepared. Radiance values in the specified bands of the satellite picture should be transformed to Top of Atmosphere (TOA) planetary reflectance values using reflectance rescaling coefficients found in the image's metadata file [18].

Conversion of Digital Numbers (DN) in to (TOA) Reflectance values:

$$\rho\lambda' = M\rho \times Qcal + A\rho \quad (1)$$

Where:

$\rho\lambda'$ = TOA Planetary Spectral Reflectance, without correction for solar angle.

$M\rho$ = Reflectance multiplicative scaling factor for the band.

$A\rho$ = Reflectance additive scaling factor for the band.

Qcal = pixel value in DN.

Correcting the Reflectance value with the Sun angle:

$$P\lambda = \rho\lambda' / \sin \theta_{SE} \quad (2)$$

Where:

$P\lambda$ = Reflectance values after sun angle correction.

$\rho\lambda'$ = TOA Planetary Spectral Reflectance.

θ_{SE} = Local sun elevation angle.

3.2.3. Surface Area Extraction

Landsat images were analyzed using the Modified Normalized Difference Water Index (MNDWI) to estimate the area of Sawa Lake and the Normalized Difference Vegetation Index (NDVI) to determine vegetation cover area for 1994, 2004, 2014, and 2024.

3.2.3.1. Modified Normalized Difference Water Index (MNDWI): This index was first presented by [19] it is a development of the NDWI proposed by [20]. It refers to the ratio of the difference between the green and Short-Wave Infrared wavelengths to their sum. Its principal application is to detect open water and map water bodies, and it may be calculated applying the equation below:

$$MNDWI = ((Green-SWIR1)) / ((Green+SWIR1)) \quad (3)$$

The MNDWI value ranges from -1 to 1. The sample type is water if (MNDWI >0) and non-water if (MNDWI ≤ 0).

3.2.3.2. Normalized Difference Vegetation Index (NDVI) This index was first presented by [21] and then developed by [22]. It refers to the ratio of the difference between the near infrared and red wavelengths to their sum. Its major

function is to monitor vegetation cover, which may be estimated using the following equation

NDVI= ((NIR-Red)) / ((NIR+Red)) (4)

The NDVI value ranges from -1 to 1. The sample type is vegetation if (NDVI >0) and Areas of barren rock, sand, or snow if (NDVI ≤ 0).

4. Results and Discussion

4.1. Water body and vegetation cover mapping

(Figure 2) Shows Sawa Lake area and vegetation cover utilizing MNDWI and NDVI. The blue hue symbolizes Sawa Lake and other water features; the green color represents vegetation cover; and the orange color represents different kinds of land cover.

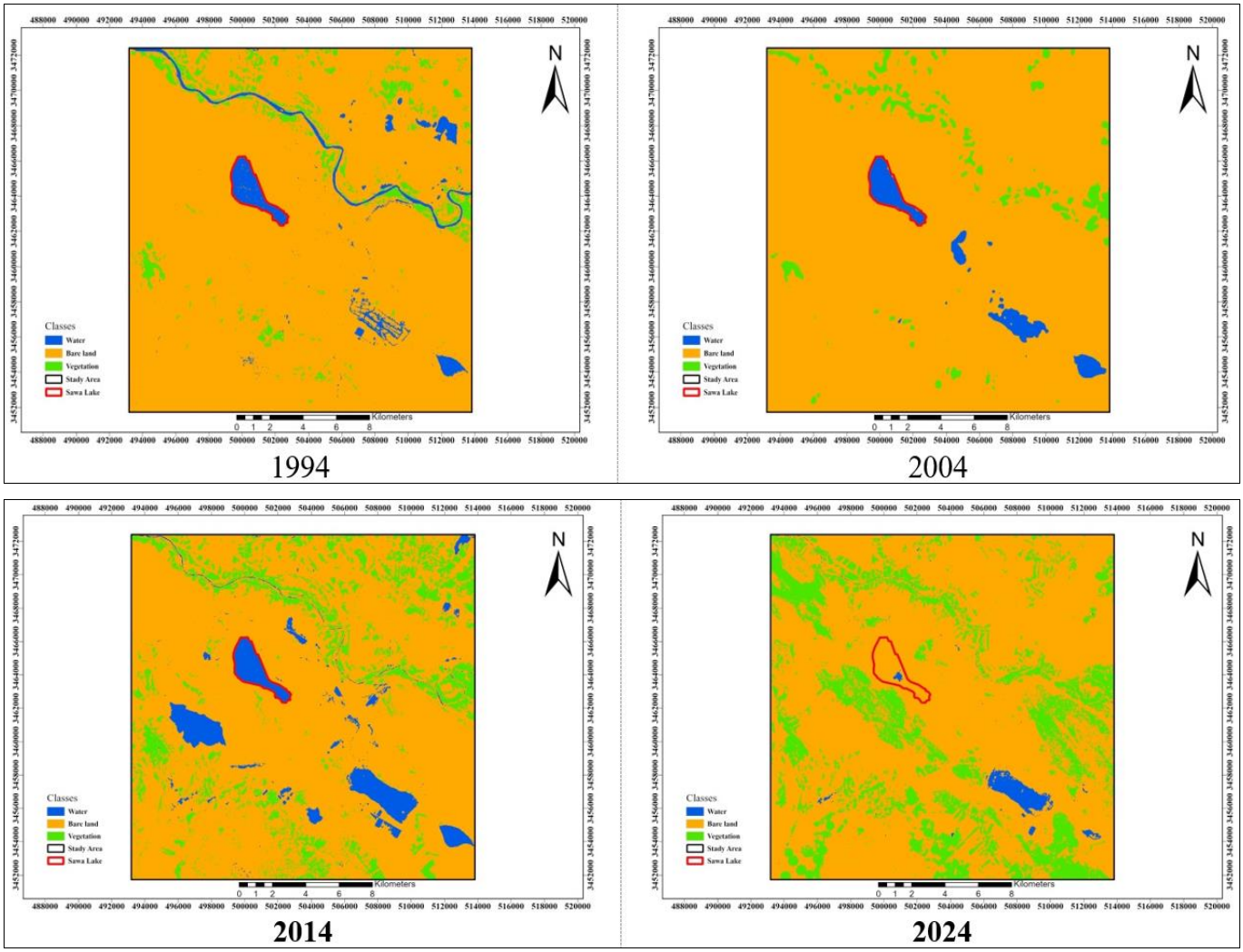

Fig 2: Shows the changes in Sawa Lake area and vegetation cover based on MNDWI and NDVI for 1994, 2004, 2014, and 2024.

4.2. Temporal Analysis

Table 2 shows the anticipated areas of Sawa Lake and vegetation cover based on the MNDWI and NDVI indicators for 1994, 2004, 2014, and 2024. Table 3 depicts the amount of change in the surface area of Lake Sawa and the adjacent agricultural fields. We can observe that between 1994 and 2014, the lake remained continuous due to a balance between the amount of groundwater injected and the amount evaporated. The lake's area decreased by over 93% between 2014 and 2024, reaching a low of 0.31 km² during the study period. The lake's surface area dropped by -4.00 km² (92% loss) between 1994 and 2024, primarily between 2014 and 2024, according to the MNDWI index readings. Vegetation cover declined by 4.26 km² from 18.87 km² in 1994 to 14.61 km² in 2004, resulting in a 22% decrease. In 2014, it increased by 34.85 km² to 49.46 km², a 238% growth. Between 2014 and 2024, it increased by 33.25 km², a 67% rise, reaching its greatest area of 82.71 km² in 2024. This increase coincided with the devastating deterioration of Lake Sawa's surface area. From 1994 to 2024, agricultural areas around the lake increased by 63.84 km², or 338%, as reflected by the NDVI index. Table 4 illustrates the amount of change that took place in climatic components over time. During the study period, all climatic parameters showed significant differences between increases and declines. Through the results of the time series analysis with a ten-year average for the period 1994-2023 and comparing it with the lake's area in the 2004, 2014, and 2024 images, we observed that the number of actual sunshine hours showed a steady upward trend, contributing to the region's rising temperatures. The lowest levels were reported between 1994 and 2003, which positively reflected the lake area in the 2004 photograph. This was followed by the period 2004–2013, during which the lake's surface area remained essentially constant in the 2014 pictures. However, the period 2014-2023 had the highest values for the number of actual sunshine hours, corresponding with the lake's decline, which had the smallest area in the 2024

photos. Temperatures likewise showed a constant upward trend, similar with the direction of actual sunshine hours, and had the same effect due to their strong association with sunlight, which associates temperature and lake area in a negative relationship. The recent increase in temperatures coincided with a decrease and deterioration in the lake's surface area. Rainfall, on the other hand, fluctuated over the course of the research. Contrary to expectations, the period 2014-2023 had the highest rainfall rate among the other eras. In contrast, the lake area declined, with the lowest area recorded in the 2024 pictures. The lowest rainfall rate was reported between 2004 and 2013, although the lake area's surface size remained reasonably stable in 2014. The same tendency can be seen in the period 1994-2003, which had a faster rate than the subsequent era, with the lake area in the 2004 photos not increasing significantly. These results show that the lake area is not related to an increase or decrease in rainfall. Relative humidity fell steadily and was negatively associated to the rise in temperatures during the research period. The highest levels were reported between 1994 and 2003, followed by 2004 to 2013. In contrast, the period 2014-2023 had the lowest relative humidity compared to the previous periods, indicating an effect opposite that of temperature. Although a decrease in humidity has a generally favorable effect on the region, it did not have a positive impact on the lake's area during its decline, demonstrating a weak association between humidity and lake area. Wind speed increased steadily, in line with temperature and negatively proportionate to atmospheric pressure. Wind speed was at its lowest between 1994 and 2003, which positively reflected the lake's area in the 2004 photos. This was followed by the period 2004-2013, when wind speeds increased slightly, but the lake's area remained unchanged in the 2014 photographs. The highest wind speed was reported during the study's last phase, from 2014 to 2023, matching with the lake's decline in 2024 photos. In contrast, air pressure fell steadily and was negatively associated to the region's increased wind speed over the study period. The greatest values were recorded between 2014 and 2023, contributing to an increase in wind speed during the same time, followed by the period 2004 to 2013, which showed a minor decline in pressure levels. In contrast, the maximum atmospheric pressure was recorded between 1994 and 2003, which coincided with a reduction in wind speed. These results show that the recent decrease in pressure on the lake's area has had an indirect negative impact.

Table 2: The area of the water body of Sawa Lake, and vegetation cover

Year	Area of Sawa Lake (km2)	Vegetation Cover Area (km2)
1994	4.31	18.87
2004	4.39	14.61
2014	4.55	49.46
2024	0.31	82.71

Table 3: The changes in water body of Sawa Lake, and vegetation cover based on MNDWI and NDVI for 1994, 2004, 2014 and 2024

Classes	Change of Area km^2							
	1994 to 2004		2004 to 2014		2014 to 2024		1994 to 2024	
	Area	%	Area	%	Area	%	Area	%
Sawa Lake	0.08	1.8	0.16	3.6	-4.24	-93	-4.00	-92
Vegetation Cover	-4.26	-22	34.85	238	33.25	67	63.84	338

Table 4: The changes in climate elements from 1994 to 2023

Climate Elements	Time Series Average			Measuring Unit
	(1994-2003)	(2004-2013)	(2014-2023)	
Actual Solar Brightness	8.49	8.80	9.17	H $^{D-1}$
Temperature Min./Max.	17.32/32.68	17.88/32.72	19.04/33.31	°c
Wind Speed	3.15	3.41	3.86	m s^{-1}
Rainfall	112.31	86.39	120.34	mm
Relative Humidity	41.36	37.73	36.27	%
Atmospheric Pressure	1010.64	1010.53	1011.37	mbar

4.3. The Influence of Climatic Elements on the Study Area

Table 5: Monthly Average of Climate Elements from 1994 to 2023

Month	Solar Brightness h d^{-1}	Temperature °C		Wind Speed m s^{-1}	Total Rainfall mm	Relative Humidity %	Atmospheric Pressure mbar
		Min.	Max.				
January	6.60	6.64	18.14	2.99	606.28	61.69	1020.4
February	7.42	8.23	21.27	3.41	390.11	53.50	1018.8
March	7.90	12.13	26.31	3.78	425.15	44.03	1014.7
April	8.25	18.23	32.42	3.84	328.15	36.76	1011.6
May	9.38	24.05	38.62	3.86	103.94	25.96	1007.8
June	11.49	27.03	43.59	4.46	0	22.16	1003.1
July	11.60	26.67	45.36	4.14	0	21.11	999.4
August	11.34	27.81	46.01	3.70	0	22.50	1000.8
September	9.75	24.33	42.13	3.35	0	25.86	1003.3
October	8.49	19.81	34.97	2.94	184.18	35.56	1012.5
November	7.38	13.23	25.83	2.85	547.82	53.30	1017.5
December	6.26	8.50	20.25	2.80	604.95	58.80	1019.8

4.3.1. Actual Solar Brightness

Table 5 demonstrates an increase in the amount of actual sunshine hours over the summer months. These hours gradually increase starting at the end of March, continue to rise through April and May, and show a large increase in June, reaching their peak in July. The high rates of sunshine hours endure throughout August and then begin to fall until reaching their lowest level in December. Due to the increase in sunshine hours during the summer, the amount of solar radiation absorbed also increases, which in turn raises temperatures. Conversely, during winter, the converse occurs. From this, it is obvious that the study area receives enormous quantities of solar energy throughout the summer due to the vertical angle of the sun's rays during this season. This leads to greater air and soil temperatures and increased evaporation, which in turn increases water losses through evaporation from water bodies and seasonal streams. Since agriculture in the study area relies on groundwater, the amount of water dragged from wells increases, and the number of wells rises to compensate for the water limited supplies.

4.3.2 Temperature

Table 5 illustrates the synchronization of minimum and maximum temperatures throughout the year throughout the study period. Temperatures begin to rise gradually with the advent of spring, notably in March, and continue to increase until the summer solstice in June. During this time, the angle of sunlight becomes nearly vertical at noon, increasing daylight hours and the number of actual sunshine hours, which in turn raises temperatures further. This rising trend in temperatures continues through July and August, which record the greatest average maximum temperatures. Afterward, temperatures steadily decline with the arrival of autumn in September, up to the winter solstice in December, where daylight hours are at their shortest, and actual sunshine hours are reduced due to gloomy skies, further decreasing temperatures. January often has the lowest average minimum and maximum temperatures. When comparing real sunshine hours reported in the research area, it becomes evident that the highest rates occur in June, July, and August, corresponding with the highest temperatures, proving a direct relationship between temperature and solar radiation. The increase in summer temperatures is mostly due to the higher angle of solar radiation and longer daylight hours, which enhance the quantity of heat absorbed during June, July, and August. This results in increased evaporation from water bodies and groundwater through capillary action, rising the demand for agricultural water, consequently diminishing groundwater levels.

4.3.3 Wind Speed

Table 5 demonstrates that wind speed starts to grow gradually from February, continuing through the spring months of March, April, and May, and culminating at the summer solstice in June. As temperatures rise, wind speeds also increase, reaching their peak levels in June and July. The wind speed then reduces slightly during August and September, with a more dramatic reduction coming in October when summer finishes, temperatures fall, and autumn begins. This declining tendency continues into November and December, where the lowest wind speeds are recorded. When comparing wind speed statistics with temperatures in the research area, it becomes obvious that greater temperatures correlate with increased wind speeds, demonstrating a direct relationship between wind speed and temperature. High wind speeds during the hot summer months significantly damage water supplies in the research location. As temperatures rise, increased wind speed promotes evaporation processes and plant transpiration, leading to higher water use. This also causes the soil's surface layer to dry out, making capillary action more effective at drawing groundwater to the surface, so depleting stored water. Furthermore, high wind speeds reduce air pressure inside wells, raising water levels and exposing them to evaporation. Wind also displaces the moist air above water bodies with dry air, increasing evaporation and water loss. These wind-driven activities, combined with the region's flat geography that allows winds to cross long distances without losing speed or changing direction, aggravate drought conditions, leading to increased groundwater withdrawal from wells and major depletion for diverse purposes.

4.3.4 Rainfall

Table 5 shows that the study area suffers from a shortage of rainfall, with changes from month to month. Most of the annual total rainfall occurs in the winter and spring seasons. Rain begins in October, increasing with the arrival of winter in November, December, and January, which recorded the most total rainfall throughout the research period. Rainfall then progressively decreases and continues to decline until May. There is no rain during the summer months (June, July, August) and even with the arrival of fall in September. Thus, the lack of rain and the rise in summer temperatures contribute to increased evaporation rates and low relative humidity, generating a water deficit when evaporation exceeds rainfall. The area's rainfall is identifiable by variation and changing quantities from one place to another, with irregular timing. It may rain in one day or month quantities equivalent to the total yearly rainfall. This form of precipitation is deemed ineffectual for recharging groundwater in the same area of precipitation. Heavy rains falling over a short period may evolve into torrents that settle in regions far from where they dropped or may fall as light showers, which expose them to evaporation as soon as they reach the surface, reducing their impact owing to soil drying.

4.3.5 Relative Humidity

Table 5 shows high relative humidity throughout the winter months (October, November, December, January, and February). When compared with temperatures, same months likewise reported their lowest rates, demonstrating an negative association between humidity and temperature. Therefore, high relative humidity coincides with lower temperatures during cold winter months, as it requires specific variables to increase, such as condensation, low temperatures, and wind speed. High relative humidity values restrict evaporation rates from water bodies and assist maintain water levels in seasonal valleys and low areas from rainfall for as long as possible, contributing to enhanced groundwater recharge. Conversely, in summer, when temperatures rise, relative humidity falls, resulting to higher evaporation.

4.3.6 Atmospheric Pressure

Table 5 shows fluctuations in atmospheric pressure values

throughout the seasons. Pressure rises in the extremely cold winter, whereas in summer, it drops progressively from February to July. It then begins to climb gradually between August and September, with a large and noticeable increase in October, continuing through November and December until January. Comparing the recorded air pressure values for the study area with temperatures, it is noted that lower pressure values coincide with higher temperatures and vice versa, demonstrating a negative correlation between atmospheric pressure and temperature. Similarly, wind speed also demonstrates an negative relationship with air pressure. Therefore, temperature controls the fluctuation in pressure values, which in turn impacts wind speed and direction. The decrease in air pressure during hot summer months significantly influences water supplies in the studied location. With rising temperatures, pressure lowers, wind speed increases, triggering evaporation processes and drying up the soil surface layer, increasing pressure on groundwater.

4.4 Analysis of Temporal Variation in the Surface Area of Sawa Lake and the Influence of Climatic Factors

Climate changes during the previous thirty years have directly or indirectly led to the deterioration of the lake region, notably in the recent time of the study. Heat and wind variables had a direct impact on the region, while brightness and pressure factors contributed indirectly by rising temperatures and increasing wind speed, respectively. Humidity and rainfall factors did not demonstrate a distinct impact on the region. Therefore, temperature is the most obvious and significant component among others, with the most impact on changing the ecosystem of the region. This correlates with worldwide climatic changes. Rising temperatures in the region reduced air pressure values and increased wind speed, influencing several features of the research area, including soil, water, and plant. High temperatures reduce the moisture of the soil surface layer, increase plant transpiration, and hence water consumption for agricultural crops. They also boost the kinetic energy of water in water bodies, raising its warmth and speed. Lower atmospheric pressure values increase wind speed, which displaces moist air over water bodies with dry air, encouraging capillary action to pull groundwater to the surface and increasing water levels in wells. This set of impacts leads to greater evaporation rates, resulting in water deficit in the region. As the region relies on groundwater for diverse agricultural, industrial, and other uses, the quantity of water withdrawn from wells has increased in recent years, altering groundwater balance and decreasing flows towards the lake.

5. Conclusion

1. The lake's surface area was constant from 1994 to 2014, but it deteriorated from 2014 to 2024, dropping severely. During that time, the lake lost more than 93% of its surface area, raising concerns that it will eventually dry up and perish.
2. Temperature was the most major changing climatic component during the study period, and it has been growing in recent years. This inclination concurs with global climate change and global warming.
3. Despite increases in rainfall levels, particularly between 2014 and 2023, rainfall had no discernible impact on the lake's surface area. In contrast, the lake's surface area shrank.
4. Climatic changes, notably recent temperature increases, have indirectly contributed to the lake's surface area deterioration by increasing water consumption for agricultural fields in the region, which has increased by 238%. Because the region relies heavily on groundwater for irrigation, the number of wells has expanded to satisfy the water shortfall, resulting in increasing water extraction rates. As a result, groundwater thresholds were decreased locally, as were levels in locations where water flowed naturally.

6. References

1. Malik A, Kumar A, Kisi O, Khan N, Salih SQ, Yaseen ZM. Analysis of dry and wet climate characteristics at Uttarakhand (India) using effective drought index. Nat Hazards. 2021;105:1643-1662. DOI: 10.1007/s11069-020-04370-5.
2. Shiru MS, Shahid S, Dewan A, Chung ES, Alias N, Ahmed K, *et al*. Projection of meteorological droughts in Nigeria during growing seasons under climate change scenarios. Sci Rep. 2020;10(1):10107. DOI: 10.1038/s41598-020-67146-8.
3. Mahdi MM, Khaleefa UQ, Shareef NF. Study of Sawa lake fauna, Holocene deposits, Al-Muthanna Province, Southern Iraq. Mesopotamian J Mar Sci. 2017;32(2):104-114. DOI: 10.58629/mjms.v32i2.65.
4. Awadh SM, Al-Sulttani AH, Yaseen ZM. Temporal dynamic drought interpretation of Sawa Lake: case study located at the Southern Iraqi region. Nat Hazards. 2022;112(1):619-638. DOI:10.1007/s11069-021-05198-3.
5. Yousuf MA, Rapantova N, Younis JH. Sustainable water management in Iraq (Kurdistan) as a challenge for governmental responsibility. Water. 2018;10(11):1651. DOI: 10.3390/w10111651.
6. Khayyun TS, Mahdi HH. Predicted climate change impact on groundwater flow for the upper zone of Iraqi aquifers. J Southwest Jiao tong Univ. 2020;55(2):1-25. DOI: 10.35741/issn.0258-2724.55.2.17.
7. Helali J, Asaadi S, Jafarie T, Habibi M, Salimi S, Momenpour SE, *et al*. Drought monitoring and its effects on vegetation and water extent changes using remote sensing data in Urmia Lake watershed, Iran. J Water Clim Change. 2022;13(5):2107-2128. DOI: 10.2166/wcc.2022.460.
8. Diaz V, Perez GAC, Van Lanen HA, Solomatine D, Varouchakis EA. An approach to characterise spatio-temporal drought dynamics. Adv Water Resour. 2020;137:103512. DOI: 10.1016/j.advwatres.2020.103512.
9. Peng Y, He G, Wang G, Cao H. Surface water changes in Dongting lake from 1975 to 2019 based on multisource remote-sensing images. Remote Sens. 2021;13(9):1827. DOI: 10.3390/rs13091827.
10. Huang X, Xie C, Fang X, Zhang L. Combining pixel- and object-based machine learning for identification of water-body types from urban high-resolution remote-sensing imagery. IEEE J Sel. Top Appl. Earth Obs. Remote Sens. 2015;8(5):2097-2110. DOI: 10.1109/JSTARS.2015.2420713.
11. Hamade JA, Dakhel FT, aldeen ali Abrahem S. Variation of water cover in Iraq (1992-2022). Nasaq.

2022;35(7):635-677. Available from: https://nasaqiraq.com/volume-35-issue-7/.
12. Radeef HA, Inbethaq M, Abdulameer A. The water area of Sawa Lake as derived from land surface temperature and remote sensing data. Ibn AL-Haitham J Pure Appl. Sci. 2023;36(1):100-112. DOI: 10.30526/36.1.2873.
13. Mousa YA, Hasan AF, Helmholz P. Spatio-temporal analysis of Sawa Lake's physical parameters between (1985–2020) and drought investigations using Landsat imageries. Remote Sens. 2022;14(8):1-19. DOI: 10.3390/rs14081831.
14. Al-Jaysha WJ, Mousa AN. Valleys and depressions in the desert of Al-Muthanna Badia - Iraq and the possibility of investing its water resources in agricultural development. Route Educ. Soc. Sci. J. 2020;7(3):584-612.
15. Hatem AJ, Al-Jasim AAN, Abduljabbar HM. A study of the climate and human impact on the future survival of the Al-Sannya marsh in Iraq. J Water Land Dev. 2021;51(X–XII):168-173. DOI: 10.24425/jwld.2021.139027.
16. Boschetti T, Awadh SM, Salvioli-Mariani E. The origin and MgCl2–NaCl variations in an athalassic sag pond: insights from chemical and isotopic data. Aquat Geochem. 2018;24:137-162. DOI: 10.1007/s10498-018-9337-y.
17. Al-Tememi MK, Al-Mosawi WM, Abdulnabi ZA. Monitoring the change of water level and its effect on water quality in Sawa Lake, Southwest Iraq. Iraqi J Sci. 2019;60(10):2177-2185. DOI: 10.24996/ijs.2019.60.10.11.
18. Samarawickrama U, Piyaratne D, Ranagalage M. Relationship between NDVI with Tasseled Cap indices: A remote sensing-based analysis. Int. J Innov Res Technol. 2017;3(12):13-19.
19. Xu H. Modification of normalized difference water index (NDWI) to enhance open water features in remotely sensed imagery. Int. J Remote Sens. 2006;27(14):3025-3033. DOI: 10.1080/01431160600589179.
20. McFeeters SK. The use of the normalized difference water index (NDWI) in the delineation of open water features. Int J Remote Sens. 1996;17(7):1425-1432. DOI: 10.1080/01431169608948714.
21. Rouse JW, Haas RH, Schell JA, Deering DW. Monitoring vegetation systems in the Great Plains with ERTS. NASA Spec Publ. 1974;351(1):309-330. Available from: https://api.semanticscholar.org/CorpusID:133358670.
22. Tucker CJ. Red and photographic infrared linear combinations for monitoring vegetation. Remote Sens Environ. 1979;8(2):127-150. DOI: 10.1016/0034-4257(79)90013-0.